The impact of aerosol vertical distribution on aerosol optical depth retrieval using CALIPSO and MODIS data

Case study over dust and smoke regions

Wu, Yerong; de Graaf, Martin; Menenti, Massimo

DOI
10.1002/2016JD026355

Publication date
2017

Document Version
Final published version

Published in
Journal Of Geophysical Research-Atmospheres

AGU PUBLICATIONS

JGR

Journal of Geophysical Research: Atmospheres

RESEARCH ARTICLE
10.1002/2016JD026355

Key Points:
- The MODIS Collection 6 algorithm (C6) AOD retrieval is sensitive to aerosol layer height
- The layer height inferred from CALIPSO data is ingested into C6 to yield a better retrieval
- Elevated smoke or dust layers can negatively bias the retrievals by 3–5% in C6

Correspondence to:
Y. Wu,
yerong.wu@tudelft.nl

Citation:
Wu, Y., M. de Graaf, and M. Menenti (2017), The impact of aerosol vertical distribution on aerosol optical depth retrieval using CALIPSO and MODIS data: Case study over dust and smoke regions, *J. Geophys. Res. Atmos. Atmos.*, *122*, 8801–8815, doi:10.1002/2016JD026355.

Received 9 DEC 2016
Accepted 22 JUL 2017
Accepted article online 26 JUL 2017
Published online 29 AUG 2017

The impact of aerosol vertical distribution on aerosol optical depth retrieval using CALIPSO and MODIS data: Case study over dust and smoke regions

Yerong Wu[1], Martin de Graaf[1,2], and Massimo Menenti[1,3]

[1]Department of Geoscience and Remote Sensing, Delft University of Technology, Delft, Netherlands, [2]Royal Netherlands Meteorological Institute (KNMI), De Bilt, Netherlands, [3]State Key Laboratory of Remote Sensing Science, Institute of Remote Sensing and Digital Earth, Chinese Academy of Sciences, Beijing, China

Abstract Global quantitative aerosol information has been derived from MODerate Resolution Imaging SpectroRadiometer (MODIS) observations for decades since early 2000 and widely used for air quality and climate change research. However, the operational MODIS Aerosol Optical Depth (AOD) products Collection 6 (C6) can still be biased, because of uncertainty in assumed aerosol optical properties and aerosol vertical distribution. This study investigates the impact of aerosol vertical distribution on the AOD retrieval. We developed a new algorithm by considering dynamic vertical profiles, which is an adaptation of MODIS C6 Dark Target (C6_DT) algorithm over land. The new algorithm makes use of the aerosol vertical profile extracted from Cloud-Aerosol Lidar and Infrared Pathfinder Satellite Observation (CALIPSO) measurements to generate an accurate top of the atmosphere (TOA) reflectance for the AOD retrieval, where the profile is assumed to be a single layer and represented as a Gaussian function with the mean height as single variable. To test the impact, a comparison was made between MODIS DT and Aerosol Robotic Network (AERONET) AOD, over dust and smoke regions. The results show that the aerosol vertical distribution has a strong impact on the AOD retrieval. The assumed aerosol layers close to the ground can negatively bias the retrievals in C6_DT. Regarding the evaluated smoke and dust layers, the new algorithm can improve the retrieval by reducing the negative biases by 3–5%.

1. Introduction

Aerosols suspended in the atmosphere are of importance on human health, cloud formation, precipitation, and climate change [*Intergovernmental Panel on Climate Change (IPCC)*, 2013]. Most of the aerosols are produced by, e.g., desert dust, forest fire, volcano ash, and industrial emissions. These aerosols can move by wind, sink by their gravity, and be removed by variable weather (e.g., precipitation and cloud formation) on a regional or the global scale. Hence, aerosol loadings and properties present a strong variability over space and time.

Many studies have been done to obtain aerosol properties with ground-based and spaceborne instruments. Observing the Earth from space, satellites have the unique advantage of large or even global coverage. Therefore, they have been extensively used to retrieve aerosol properties, such as the single viewing satellite sensor MODerate Resolution Imaging SpectroRadiometer (MODIS) [*Remer et al.*, 2005; *Levy et al.*, 2007a, 2013; *Hsu et al.*, 2004, 2006, 2013; *Sayer et al.*, 2013, 2015, 2016], the advanced very high resolution radiometer (AVHRR) [*Stowe et al.*, 1997; *Mishchenko et al.*, 1999], multiangle viewing sensor Advanced Along-Track Scanning Radiometer (AATSR) [*North*, 2002; *North et al.*, 1999; *Grey et al.*, 2006; *Thomas et al.*, 2009], multiangle Imaging Spectroradiometer (MISR) [*Martonchik et al.*, 1998, 2002, 2009; *Keller et al.*, 2007], PoLarization and directionality of the Earth's Reflectances (POLDER) [*Tanré et al.*, 2011; *Herman et al.*, 2005; *Dubovik et al.*, 2011], and active detection sensor Cloud-Aerosol Lidar and Infrared Pathfinder Satellite Observation (CALIPSO) [*Z. Liu et al.*, 2008; *D. Liu et al.*, 2008].

For characterizing aerosol concentration and evaluating the impacts of aerosols on climate change, aerosol optical depth (AOD) has gained a lot of attention from the scientific community. This is because AOD can be applied to indicate aerosol amount or particulate matter mass near the surface to monitor air quality [e.g., *Chu et al.*, 2003; *Engel-Cox et al.*, 2004; *Nicolantonio et al.*, 2007; *Hoff and Christopher*, 2009; *Wu et al.*, 2012;

Guo et al., 2016]. It also can be used to estimate the aerosol cooling effects [e.g., *Kaufman et al.*, 2002; *Myhre*, 2009; *IPCC*, 2013; *Xu et al.*, 2016].

MODIS AOD product has been proven to be "state of the art" after several generation developments [*Remer et al.*, 2005; *Levy et al.*, 2007a, 2007b, 2013; *Hsu et al.*, 2004, 2006, 2013] and extensive and rigorous validations against ground measurements [e.g., *Levy et al.*, 2005, 2010; *Sayer et al.*, 2013; *Tao et al.*, 2015]. This product has been widely applied for scientific research. However, the MODIS AOD over land (e.g., Collection 6 Dark Target (C6_DT) AOD) still has a large uncertainty with the expected accuracy envelope $\pm(0.05 + 15\%)$.

The uncertainty of MODIS AOD product over land is caused by many reasons. From previous papers, we already know that surface reflectance and aerosol model choices are a source of uncertainty [e.g., *Li et al.*, 2009; *Kokhanovsky et al.*, 2010; *Lyapustin et al.*, 2011a; *Kokhanovsky et al.*, 2015; *Wu et al.*, 2016a, 2016b]. However, other issues may need more attention such as aerosol vertical distribution.

The distribution of aerosols in the atmosphere can be very diverse and be different at different vertical levels. Different distributions for aerosol layers have been applied in a number of studies. For example, the Gaussian distribution was applied in the Deep Blue AOD algorithm [*Hsu et al.*, 2004], for typical smoke to retrieve the layer height [*Lee et al.*, 2015], and for POLDER aerosol retrieval algorithm [*Dubovik et al.*, 2011], whereas exponential distribution was applied for all aerosol models in the MODIS DT AOD algorithm over land [*Levy et al.*, 2007a]. Since a fixed vertical profile was used in the MODIS algorithm that assumed most aerosols (78%) statically distributed below 3 km globally, this may give a significant bias in the AOD retrieval for the elevated aerosol layer. Through a sensitivity study, *Wu et al.* [2016a] demonstrated that for elevated smoke or dust layers (e.g., altitude = 7 km), the MODIS C6_DT algorithm can negatively bias the AOD retrievals by >10%. The Cloud-Aerosol LIdar with Orthogonal Polarization (CALIOP), flying as one of A-train instruments, can provide information on aerosol vertical profile that may be used to refine the AOD retrieval in the MODIS (Aqua) algorithm.

In this study, we developed a new algorithm (called Gau_DT) to retrieve the AOD by considering a dynamic aerosol profile with the synergistic use of MODIS and CALIPSO data. The inferred aerosol vertical profile from CALIPSO data is parameterized into the algorithm to generate an accurate top of the atmosphere (TOA) reflectance for the AOD retrieval. Section 2 introduces the Gau_DT algorithm, including the investigation of the relationship between the profile and TOA reflectance, as well as the discussion on the sensitivity of the AOD retrieval to the variation of the profile. Section 3 introduces the data collected by AERONET, MODIS, and CALIPSO and the derivation of aerosol vertical distribution from the CALIPSO data. Section 4 provides case studies (smoke and dust aerosol) to show the impact of aerosol vertical distribution on the AOD retrieval with the comparison between Gau_DT and C6_DT AOD. Conclusions are presented in section 5.

2. Method

2.1. Basic Algorithm

Many studies show improvements in DT algorithm [e.g., *Lyapustin et al.*, 2011a, 2011b; *Wu et al.*, 2016b]. However, few are global and/or time efficient. We make use of the C6_DT version [*Levy et al.*, 2013] as a reference to develop our new algorithm since this version has been found to be mature and widely accepted by the community. Here we briefly review the C6_DT AOD retrieval. In C6_DT, the radiance observed by the satellite (TOA radiance) is represented as the sum of two parts: one part due to the atmosphere scattering and the other due to the net interaction between the surface and the atmosphere. Through normalization (radiance converted to reflectance), the TOA reflectance can be written as [*Kaufman et al.*, 1997]

$$\rho^*_\lambda(\theta_0,\theta,\phi) = \rho^a_\lambda(\theta_0,\theta,\phi) + \frac{F_{d\lambda}(\theta_0)T_\lambda(\theta)\rho^s_\lambda}{1 - s_\lambda\rho^s_\lambda}, \tag{1}$$

where θ_0, θ, and ϕ are the solar zenith angle, the viewing zenith angle, and the relative azimuth angle between solar azimuth and viewing azimuth angle, respectively; λ indicates the wavelength; ρ^a_λ is the atmospheric reflectance; $F_{d\lambda}$ is the downward transmission; T_λ is the upward transmission; and s_λ is the atmospheric backscattering ratio. Except for surface reflectance ρ^s, the other four parameters ρ^a, F_d, T, and s in equation (1) are precalculated and stored in a look-up table (LUT), indexed as dimensions of aerosol type, aerosol vertical distribution, aerosol loading (τ), and geometrical illumination and viewing angle.

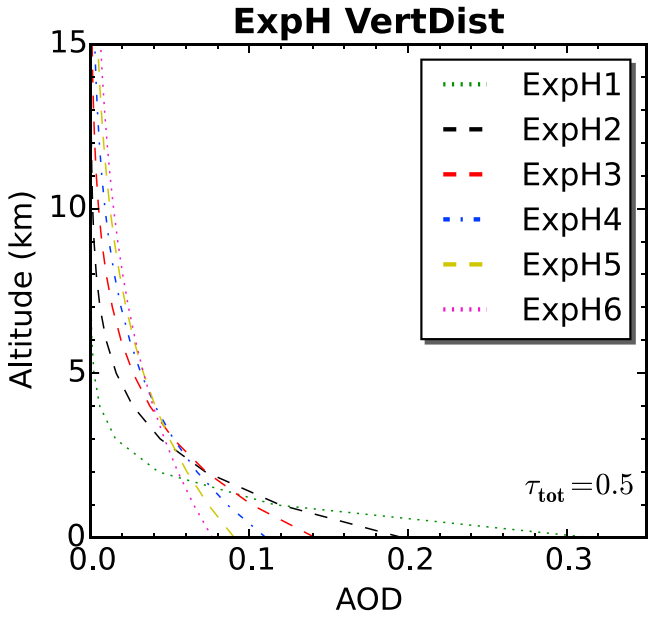

Figure 1. Exponential distribution with different scale of height. The scale of height ranges from 1 to 6 km by step of 1 km (see Table 1), where ExpH2 is applied in MODIS C6 algorithm. The total AOD τ_{tot} is set as 0.5. Here the distributions at higher (>15 km) altitude are not shown due to small values of AOD. Reproduced with permission from *Wu et al.* [2016a]. Copyright 2016 MDPI.

Regarding the mixture of fine (e.g., smoke) and coarse particles (dust), the total spectral ρ_λ^{tot*} at the top of the atmosphere is calculated by linearly mixing the spectral TOA reflectance (ρ_λ^{f*}) in fine-aerosol-dominated atmosphere and the one (ρ_λ^{c*}) in coarse-aerosol-dominated atmosphere, i.e.,

$$\rho_\lambda^{tot*} = \eta\rho_\lambda^{f*} + (1-\eta)\rho_\lambda^{c*}, \qquad (2)$$

where η is the mixing ratio defined as the ratio of the fine AOD τ_λ^f to the total AOD τ_λ^{tot} [*Remer et al.*, 2005]. The parameter τ_λ is spectrally dependent; hereafter we use τ at 0.55 μm, unless specified otherwise. Note that the linear mixing method is only applied for a "dark surface" ($0.0 < \rho_{2.11}^s < 0.25$, procedure A in C6_DT).

Over a dark surface, the MODIS C6_DT algorithm retrieves AOD τ, fine ratio η, and the 2.11 μm surface reflectance $\rho_{2.11}^s$, by fitting the simulated reflectance with the MODIS measurement at three bands (0.466, 0.644, and 2.11 μm).

The aerosol vertical distribution and its parameterization in the new algorithm are detailed in the next sections.

2.2. Aerosol Vertical Distribution

Aerosol layer can be represented as Gaussian and exponential function, as well as power law and random function. To reduce the number of the distributions, we classified them into two groups based on their characteristics. Exponential and power law functions are sorted into one group, because both of them indicate more aerosols in the lower boundary layer and less in the upper boundary layer. Random and Gaussian distribution are sorted into another group. Random distribution with a limited geometric thickness (e.g., 2 km) to some degree can be viewed as a homogeneous layer and thus can be approximately represented as a Gaussian function. Thus, exponential and Gaussian distributions were selected for analysis.

The vertical profile (layer shape and altitude) is controlled by one or two variables in the selected distributions such as a scale height h in exponential distribution and the mean height μ and the thickness σ of the aerosol layer in Gaussian:

$$\tau_{\lambda,z_i} = \tau_\lambda \left(e^{-z_i/h} - e^{-z_{i+1}/h}\right), \qquad (3)$$

$$\tau_{\lambda,z_i} = \tau_\lambda \frac{1}{\sqrt{2\pi}} \left(e^{-(z_i-\mu)^2/2\sigma^2} - e^{-(z_{i+1}-\mu)^2/2\sigma^2}\right), \qquad (4)$$

where z_i is an altitude of the ith aerosol layer.

Figure 1 shows the exponential distributions with the scale height h ranging from 1 to 6 km by step of 1 km. By increasing the scale height, more aerosols are distributed to a higher level in the atmosphere. Note that the exponential distribution with $h = 2$ (labeled as "ExpH2") is applied in the C6_DT algorithm.

For the Gaussian distribution, aerosol layers are assumed to have a limited thickness, where the aerosol particles are truncated into the interval of Gaussian 2σ. We note that with a low mean height (e.g., $\mu = 0$ km) the Gaussian distributions will give some aerosols below the surface. This is invalid for the real case. To avoid this situation, we keep the aerosols above the surface and remove the aerosols below the surface, but the total

Table 1. Gaussian (Gau1 → Gau6 and GauH0 → GauH10) and Exponential Distributions (ExpH1 → ExpH6) of Aerosol Layers Varying With the Mean Height μ or the Height Scale h[a]

Name	μ or h (km, Depending on Distribution)	σ (km)	Resolution (km)
Gau1	0	0.5	0.5
Gau2	0	1.0	0.5
Gau3	0	1.0	1.0
Gau4	3	0.5	0.5
Gau5	3	1.0	0.5
Gau6	3	1.0	1.0
GauH0	0	1.0	1.0
GauH1	1	1.0	1.0
…	…	…	…
GauH10	10	1.0	1.0
ExpH1	1	—	1.0
ExpH2	2	—	1.0
…	…	…	…
ExpH6	6	—	1.0

[a]The geometric thickness σ of the layers is applicable for Gaussian distributions. An em dash indicates the missing value for exponential distributions. Considering the limited aerosol-atmosphere layers in RT code, vertical resolutions of 0.5 and 1.0 km for the layers are also given.

amount of aerosol is still kept the same as other normal cases (e.g., $\mu >= 3$). Additionally, the vertical resolution of the aerosol layer is also taken into account since the resolution can change the layer shape. Six kinds of Gaussian distributions (Gau1 → Gau6) are given in Table 1 and shown in Figure 2. They differ in three variables: mean height (0 and 3 km), geometrical thickness (0.5 and 1 km), and vertical resolution (0.5 and 1 km).

2.2.1. The Relationship Between the TOA Reflectance and Aerosol Vertical Distribution

To parameterize the aerosol vertical profile into the algorithm, the relationship between the TOA reflectance and aerosol vertical profile needs to be quantified. Since the TOA reflectance is nearly nonsensitive to the aerosol vertical profile at long wavelengths (e.g., 0.644 and 2.12 μm) [*Wu et al.*, 2016a], we focused on the variation of the TOA reflectance at a short wavelength (0.466 μm) to the different profiles including six Gaussian (Gau1 → Gau6) and six exponential distributions (ExpH1 → ExpH6) (see Table 1).

Figure 3 presents the simulated 0.466 μm reflectance at TOA with Gaussian distributions (Gau1 → Gau6). Smoke and dust models were used. The TOA reflectance is nearly nonsensitive to the shape of the aerosol vertical distribution such as the geometrical thickness and vertical resolution of the aerosol layer, while it shows high sensitivity to the mean height. The result with exponential distributions is similar (not shown here). A similar result was also demonstrated in *Lee et al.* [2015]. We found that the TOA reflectance with dust model presents less variation with the mean height than with smoke model. This is because dust is less absorbing than smoke.

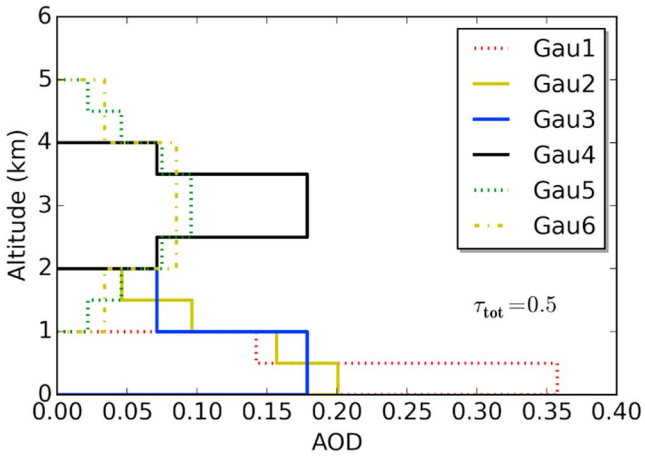

Figure 2. Discrete Gaussian distributions. The distributions shown in the figure is also given in Table 1. The total AOD τ_{tot} is set as 0.5.

Since the mean height is a major factor that influences the TOA reflectance, it is expected that the TOA reflectance with Gaussian distribution is similar to the one with exponential distribution

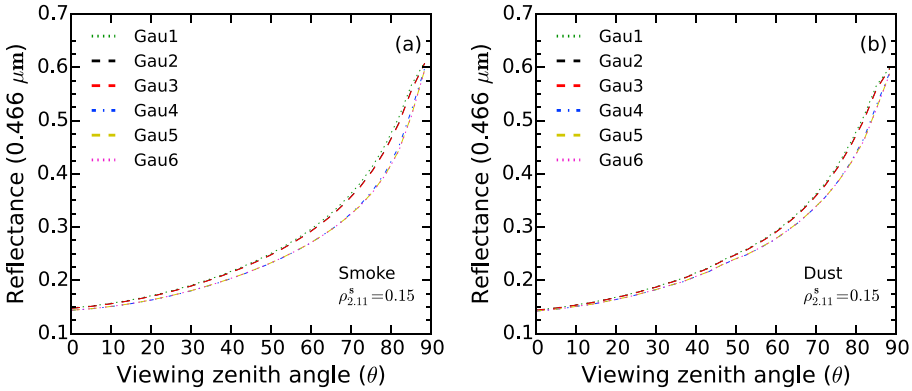

Figure 3. The TOA reflectance at 0.466 μm when the Gaussian distributions "Gau1-6" are used. The definition for these distributions is also shown in Table 1. The reflectance is calculated with (a) smoke and (b) dust model with a given solar zenith angle $\theta_0 = 48°$ and relative azimuth angle $\phi = 180°$, AOD (0.5), and surface reflectance $\rho^s_{2.11} = 0.15$. We assume that one-quarter and one-half ratio are for the surface reflectance ratio of 0.466/2.11 and 0.644/2.11.

when their mean heights are equal. To prove this, we simulated the TOA reflectance with one exponential ExpH2 and two Gaussian distributions ($\mu = 0$ and $\mu = 3$, labeled as "GauH0" and "GauH3," respectively).

Figure 4 illustrates the TOA reflectance with the three distributions (ExpH2, GauH0, and GauH3), given as a function of viewing angles. From this figure, we can see that the ExpH2 reflectance mostly falls within

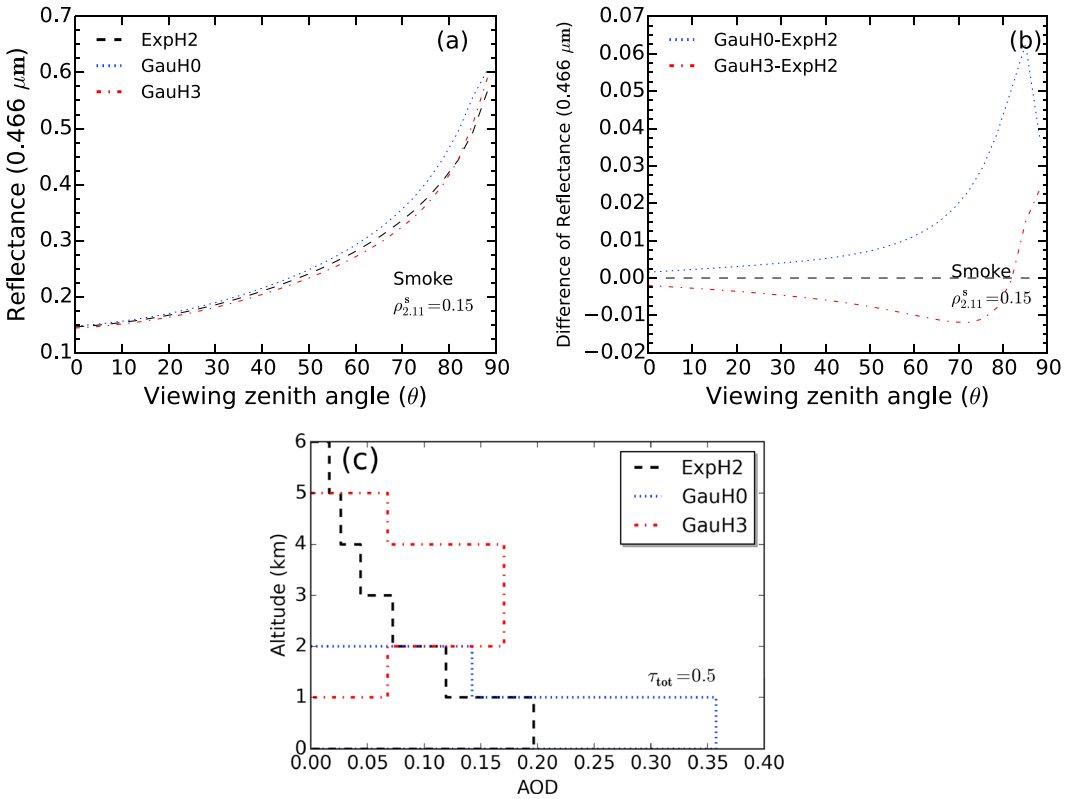

Figure 4. The TOA reflectance at 0.466 μm with exponential and Gaussian distributions. All the Gaussian distributions have the same geometrical thickness $\sigma = 1$ km and vertical resolution (1 km). "GauH*x*" means the Gaussian distribution with the mean height of *x* km. ExpH2 indicates the exponential function with the scale height of 2. (a) The TOA reflectance as a function of viewing zenith angle. (b) The difference of the TOA reflectance (e.g., "GauH0 − ExpH2"), where the dashed line means zero difference. (c) The discrete distributions. Other symbols are similar to those in Figure 3.

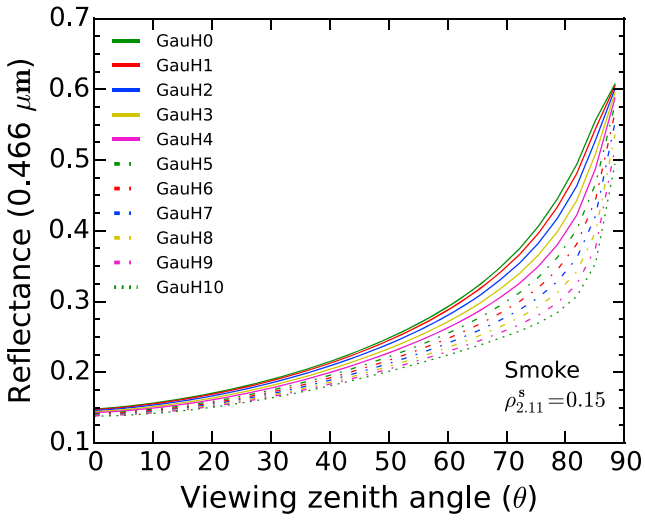

Figure 5. The TOA reflectance at 0.466 μm with different mean height (0–10 km, GauH0 → GauH10 in Table 1). Other symbols are similar to those in Figure 4.

the envelope of the GauH0 and GauH3 reflectance. Note that in ExpH2 distribution the mean height is $-2\ln(0.5) = 1.4$ km (between 0 and 3 km). Nevertheless, with a large viewing angle (e.g., $\theta_v > 80°$), the TOA reflectance with ExpH2 distribution is less than that with GauH3. This is mainly due to a different vertical slant path depending on layer/height thickness in the calculation of radiative transfer.

To further clarify the relationship between the layer mean height and the TOA reflectance, Gaussian distribution is selected for the aerosol layer where both the geometrical thickness σ and the vertical resolution of the layer are fixed at 1 km. Since the layer can climb up to higher altitude such as the dust layers that can reach 3 to 6 km in North Africa and Arabian Peninsula [*D. Liu et al.*, 2008; *Huang et al.*, 2015], we extend the mean height to a wider range (e.g., 0–10 km) for analysis.

Figure 5 presents the TOA reflectance with the Gaussian distributions where the smoke model is used. With a given geometrical viewing, the TOA reflectance presents an approximately linear decrease as increasing the altitude of aerosol layer. This is due to the fact that more isotropic scattering reflected by the Rayleigh layer is attenuated by the aerosol layer.

In summary, the TOA reflectance is highly sensitive to the mean height of the aerosol layer and nearly nonsensitive to the layer shape. Further, with the increase of the mean height, the TOA reflectance presents a linearly decreasing trend.

2.3. The Sensitivity of the AOD Retrieval to Aerosol Vertical Distribution

2.3.1. Experiment Setup

Wu et al. [2016a] demonstrated that the AOD retrieval is affected by different aerosol vertical profiles. Nevertheless, the dependence of the retrieval on the layer mean height was not fully evaluated and needs to be further clarified for our study. To address this, we designed a synthetic experiment in which the TOA reflectance was simulated with Gaussian distributions using off-line LUTs. Four mean heights (0, 3, 6, and 9 km) were set for the distribution (labeled as GauH0, GauH3, GauH6, and GauH9). The MODIS C6_DT algorithm over land (procedure A) is used in this experiment.

The experiment is extensively evaluated with aerosol properties and the observation and illumination geometries (880 geometrical combinations: $\theta_0 < 48°$, $\theta \le 60°$, and $\phi \le 180°$). Three fine mode aerosols including absorbing (smoke, $\omega_0 = 0.87$), moderately absorbing (generic, $\omega_0 = 0.92$), and nonabsorbing aerosols (urban-industrial, $\omega_0 = 0.95$), and one coarse model aerosol dust ($\omega_0 = 0.95$) [*Levy et al.*, 2007b] were used, with seven aerosol loadings (0.0, 0.25, 0.5, 1.0, 2.0, 3.0, and 5.0) and five fine ratios (0, 0.2, 0.5, 0.8, and 1). The 2.11 μm surface reflectance $\rho^s_{2.11}$ was assumed to be 0.15. The ratios of the spectral surface reflectance are given as 0.25 and 0.5 for 0.466 and 0.644 μm versus 2.11 μm, respectively.

For the evaluation of AOD errors, we use the C6_DT AOD as the reference value instead of the truth. This is because there are some intrinsic errors in the algorithm [*Levy et al.*, 2007a; *Kokhanovsky et al.*, 2010; *Wu et al.*, 2016a]. The relative error or difference of AOD retrievals $\delta(\tau)$ is defined as

$$\delta(\tau) = \frac{\tau - \tau_{\text{ref}}}{\tau_{\text{ref}}}, \tag{5}$$

where τ_{ref} indicates the reference τ which is given as the retrieval when the ExpH2 TOA reflectance is simulated. The experiment results are described by averaging 880 geometrical combinations.

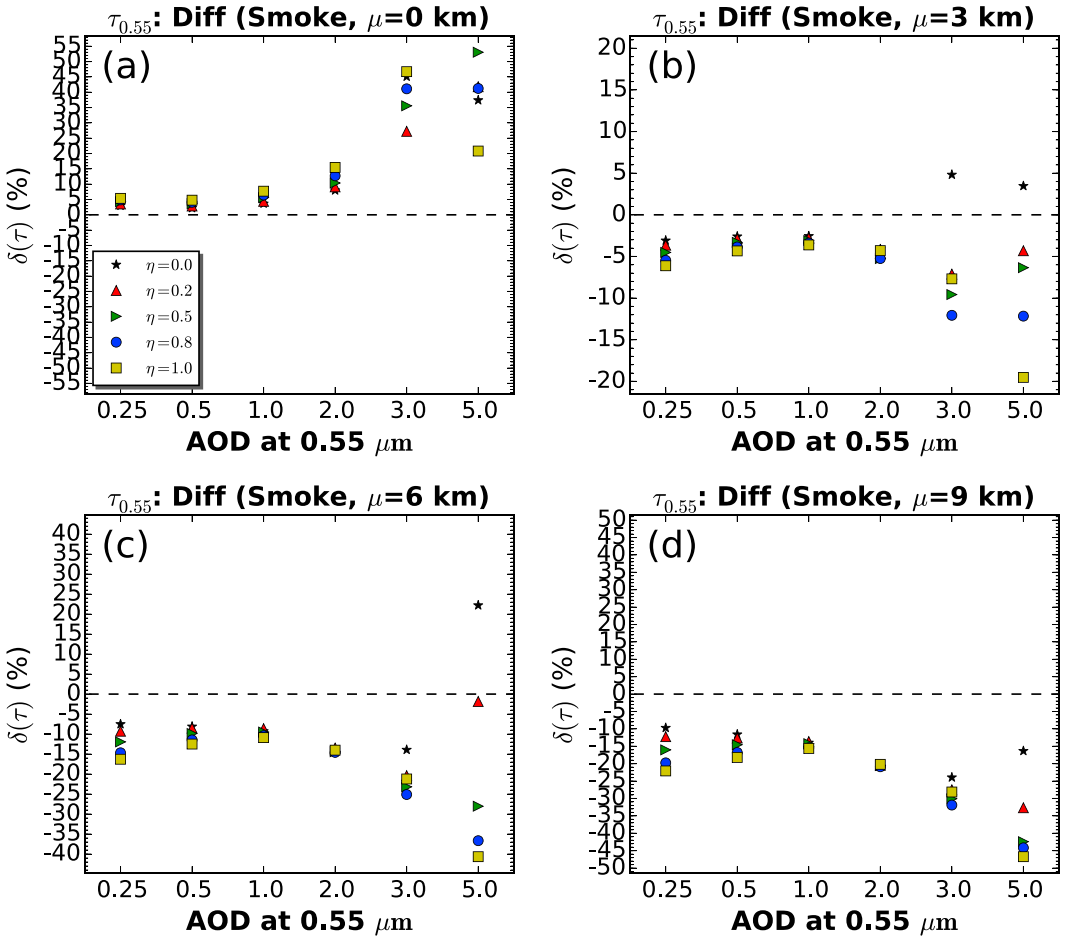

Figure 6. The errors $\delta(\tau)$ of AOD retrievals with different vertical distributions: (a–d) μ = 0, 3, 6, and 9 km. Smoke model is used in the experiment. The mean differences $\delta(\tau)$ are calculated by averaging over 880 geometrical combinations, shown as a function of aerosol loadings and fine ratios.

2.3.2. Experiment Results

Figure 6 presents the AOD errors with the four simulations (GauH0, GauH3, GauH6, and GauH9), where the ExpH2 LUT is used in the retrieval procedure. The result with smoke mixtures is shown in the figure, whereas the results with other mixtures are not given due to their generally small errors ($\delta(\tau) < 10\%$). The AOD errors are highly dependent on the mean height. Specifically, the simulation with a low aerosol layer (GauH0) gives an overestimation of the AOD retrieval. By contrast, the simulation with a high layer (GauH3, GauH6, and GauH9) causes an underestimation. In addition, the underestimation becomes even larger when a higher layer (e.g., GauH6 and GauH9) is used in the simulation. Furthermore, the error increases with increasing AOD. With AOD $\leq$2.0, the errors are limited to 5–20% , whereas the errors increase by >10% when AOD $\geq$3.0. With the increase of aerosol loading, the errors with dust model ($\eta = 0$) do not steadily increase as that with other pure fine models. This points to possible issues with the scattering phase function of the dust model.

2.4. New AOD Retrieval With Dynamic Aerosol Vertical Distribution

The experiment suggests that dynamic profile for aerosol layer has a significant impact on the AOD retrieval. To investigate this impact, we developed a new algorithm (Gau_DT) by parameterizing the profile into the retrieval. In this algorithm, the LUT is precalculated with a known vertical profile which is simply described as the Gaussian distribution, with the mean height μ as single variable. The geometrical thickness σ and the vertical resolution are fixed at 1 km for the distribution. To avoid too many LUTs applied that would consume a huge memory, three basic LUTs were prepared with the layer mean height of 0, 3, and 6 km. The LUTs will be further linearly interpolated or extrapolated to the measured mean height in the retrieval. The measurements are extracted from MODIS level 2 product "Mean_Reflectance_Land" (MYD04_L2), which is obtained through gas correction, cloud and water mask, and dark target filtering, reported at 10 × 10 km. As for the mean height,

we derived this parameter from CALIPSO data. More details of MODIS and CALIPSO data are introduced in the next section, as well as the derivation of the mean height. AERONET measurements are also introduced as ground truth data of AOD.

3. Data

3.1. AERONET Measurements

The sun photometers of AERONET provide a data set of spectral AOD at wavelengths (0.34, 0.38, 0.44, 0.67, 0.87, and 1.02 μm) retrieved from observations of the extinction of direct solar radiation under cloud-free condition. This data set is a high quality (~0.01–0.02 uncertainty) AOD with high temporal resolution (every 15 min or more often) and is extensively used for the validation of satellite AOD products [e.g., *Levy et al.*, 2010; *Kahn et al.*, 2010; *Carboni et al.*, 2012; *Sayer et al.*, 2012, 2013; *Tao et al.*, 2015]. Collected from the AERONET Version 2.0 Level 2 that are quality-assured, cloud screened, and calibrated data, the spectral AOD is reported at 0.55 μm using the method of quadratic fitting on log scale [*Eck et al.*, 1999] and used to evaluate the accuracy of satellite AOD retrievals.

3.2. MODIS Data

Two MODIS sensors, one on Terra and the other on Aqua, are observing the TOA radiance at 36 channels, with a wide swath of 2030 × 1354 km in resolutions of 250 m to 1 km (depending on channels and sensor viewing angle). Terra and Aqua have an equator crossing time of 10:30 and 13:30, respectively, monitoring the Earth daily with nearly global coverage. MODIS Aqua data are used here because CALIPSO and MODIS Aqua belong to the A-Train constellation, observing the same place at the nearly same time.

3.3. CALIPSO Data

CALIOP is a lidar instrument on board the CALIPSO satellite. It detects the vertical profile of atmospheric backscatter at 532 and 1064 nm, collecting information on cloud and aerosols and providing the data since June 2006. The original resolution of the data is 30 m vertical and 333 m horizontal before the calibration.

CALIPSO Levels 1 and 2 data are produced by CALIPSO science team [*Winker et al.*, 2006; *Vaughan et al.*, 2005]. The Level 1 data are the measurements of attenuated backscatter coefficients at 532 and 1064 nm after instrument calibration. By considering that the weaker signals are received from the higher atmospheric layers, an onboard averaging method was developed which provides full (lower) resolution in the lower (higher) atmosphere such that resolution of 30 m is only up to 8 km altitude [*Winker et al.*, 2006]. The Level 2 data provide users with the vertical features and properties of cloud and aerosols. One of the Level 2 products, vertical feature mask (VFM), is generated from the Level 1 data with the feature finder algorithm that detects and determines cloud and aerosol layers [*Vaughan et al.*, 2005]. We use the VFM data for the detection of aerosol layer. More details about this are introduced in the next section.

Figure 7a shows a sample plot of total attenuated backscatter at 532 nm observed during daytime using CALIPSO Level 1 data (data set: "Total_Attenuated_Backscatter_532"). Figure 7b presents vertical feature mask observed at the same time and place, using CALIPSO Level 2 VFM data (data set: "Feature_Classification_Flags"). In this figure, several types are determined such as clear air, cloud, aerosol, and the surface. Combining Figures 7a and 7b, it is apparent that the most attenuated backscatter is determined as "cloud" (white color in Figure 7a and cyan color in Figure 7b), whereas the moderately attenuated backscatter is determined as aerosol (orange color in Figure 7b). Note that there is no signal (black color) below the cloud in Figure 7b.

3.4. The Derivation of Aerosol Vertical Distribution (Layer Mean Height)

The mean height of aerosol layer is derived from Level 2 VFM product in two steps (also see Figure 8):

Step 1. In this step, clear air and aerosol layers are to be determined further within a window of 0.5 × 10 km (16 × 30 pixels in VFM data). An extraction method was developed for these two kinds of layers. This method searches and counts aerosol pixels from the top to the bottom of the vertical column. The window that has more than 50% aerosol pixels will be assigned as "aerosol." If it is not the case, we count clear air pixel numbers. The window that has more than 50% clear air pixels will be assigned as "clear air"; otherwise, it is given as "blank." In the search process, aerosol pixels are always first detected in the column, then clear air pixels. If there is no aerosol pixel found, then the whole column is assigned as blank.

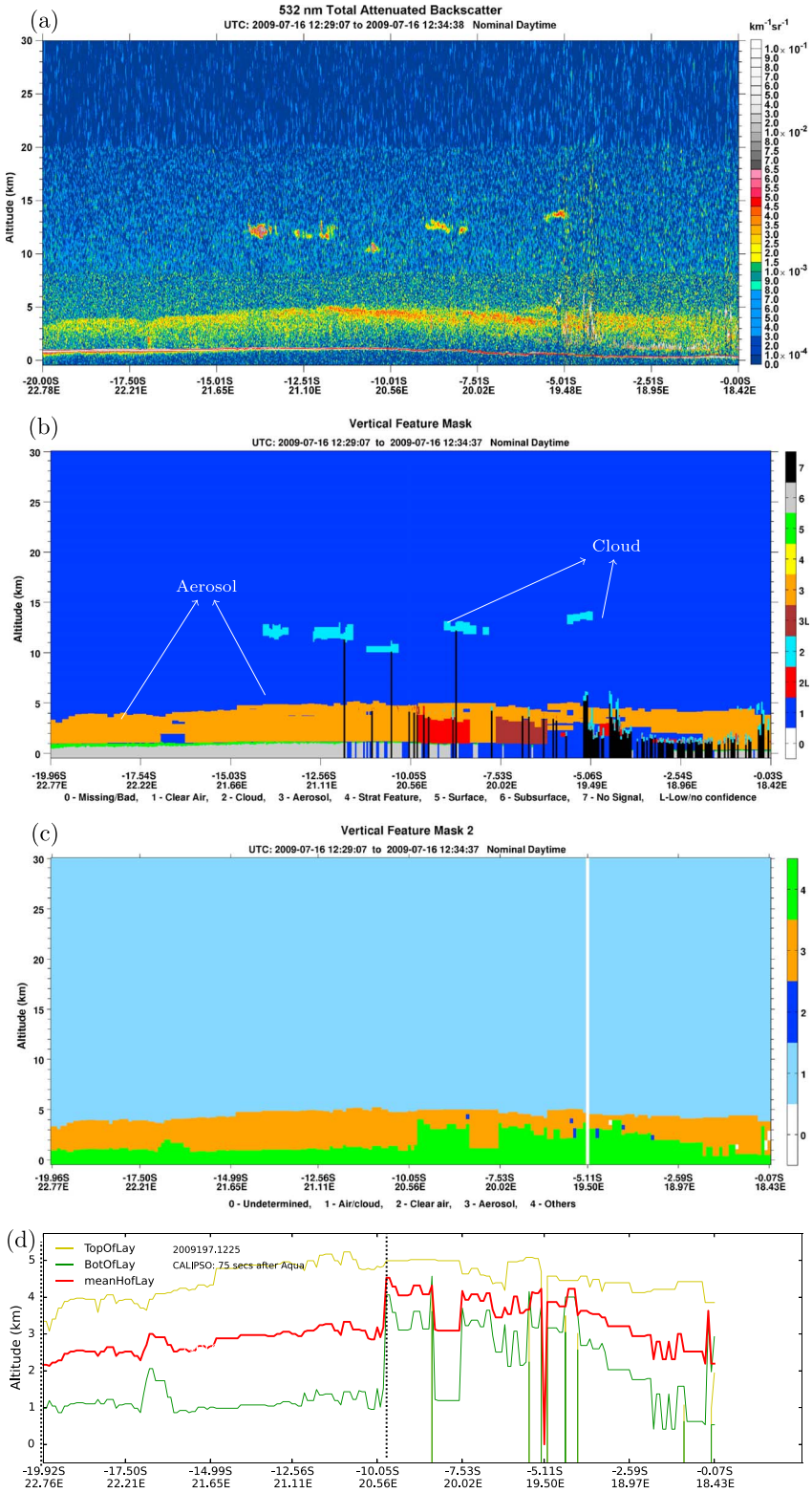

Figure 7. Atmosphere vertical profile measured by CALIPSO. The data are captured on 16 July 2009 during daytime. It is shown as Figures 7a–7d, based on the different process levels. (a) The total attenuated backscatter at 532 nm (data from CALIPSO Level 1). (b) The vertical feature mask (data from CALIPSO Level 2 vertical feature mask), where several types are classified such as cloud, clear air, and aerosol. (c) The result of types (aerosol, cloud, and clear air) after the aggregation of CALIPSO Level 2 data. (d) The aerosol layer boundary (top: yellow, bottom: green) and mean height (thick red), respectively. The two dashed lines (black) in Figure 7d indicate the region in Figure 10.

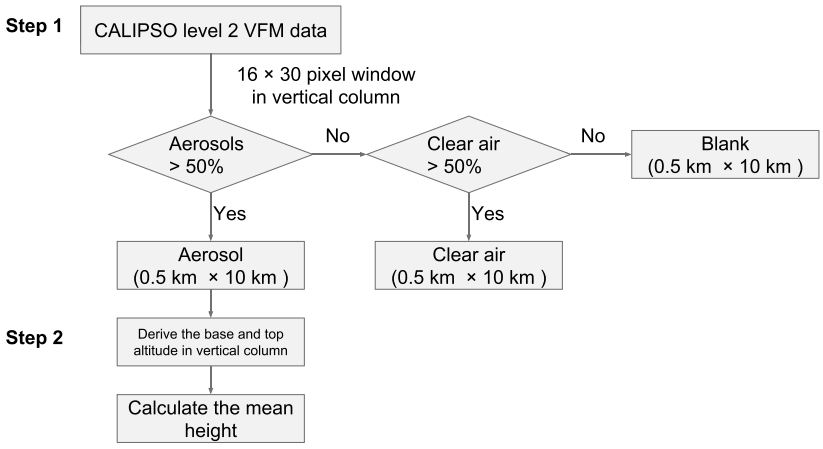

Figure 8. Flowchart for the derivation of aerosol layer mean height using CALIPSO Level 2 (VFM) data.

Step 2. Aerosol layer boundary and the layer mean height are extracted. In each vertical column with a width of 10 km, the top and base height of each aerosol layer are detected. The layer mean height is calculated by averaging the height of the top and base. Aerosol vertical profile is assumed to be a single layer.

Figure 7c illustrates the vertical feature mask with Step 1. Four types are given in the figure. They are air/cloud, clear air, aerosol, and others (could be surface, air, cloud, or a mixture of them). The undetermined area (white color) indicates that there is no aerosol found in the column. Figure 7d shows the boundary and mean height of the aerosol layer after Step 2.

Due to the nadir view only of CALIPSO, the derived height has a narrow swath (30 m). To solve the mismatch between MODIS (10 km) and aerosol height data, we resampled the height data into seasonal ($5 \times 5^{\circ}$) and real-time data sets (10×10 km), respectively. The seasonal data set is obtained by averaging the height data over a season, whereas the real-time data set is obtained by assuming the height to be homogeneous across the CALIPSO track and extending it to the whole MODIS swath (2030 km). These two data sets are used for the new algorithm. We note that the assumptions of single layer and horizontal homogeneity for the aerosol profile can hold well for the cases of a long-range pollution of dust or smoke since the aerosol layers tend to be homogeneous [*Lee et al.*, 2015]. It may not hold well for the cases that have complicated atmospheric conditions. In addition, zero values for the layer height could happen under a clear sky. For this case, we use the mean height of ExpH2 (1.4 km) instead.

4. Results and Discussions

Gau_DT was applied to smoke and dust regions. Cases of light moderately absorbing and nonabsorbing aerosols are not discussed here. This is because for these cases the impact can be easily covered by some other potential errors that could arise from instrument measurement uncertainty (e.g., calibration and random errors in channels) and from the inappropriate assumptions on the aerosol model and the relationship of surface reflectance for visible versus short wave Infrared wavelengths. Through a sensitivity analysis, *Levy et al.* [2007a] demonstrated that 3–5% errors (mean square error) of the retrieval could be accounted for by the errors of MODIS measurements or the spectral surface reflectance (presented in *Levy et al.* [2007a, Table 4b]), and would be even larger by combining these two source errors. These errors are comparable to the ones due to the aerosol dynamic vertical distribution when moderately absorbing (generic) and nonabsorbing (urban-industrial) aerosols are observed especially under light aerosol loading (e.g., AOD).

Table 2. Information of Smoke and Dust Regions

Region	Period	Geoinformation
Middle Asia (dust)	2008–2010	15°–30°N, 70°–93°E
Middle Africa (smoke)	2008–2010	20°S–0°, 10°–40°E

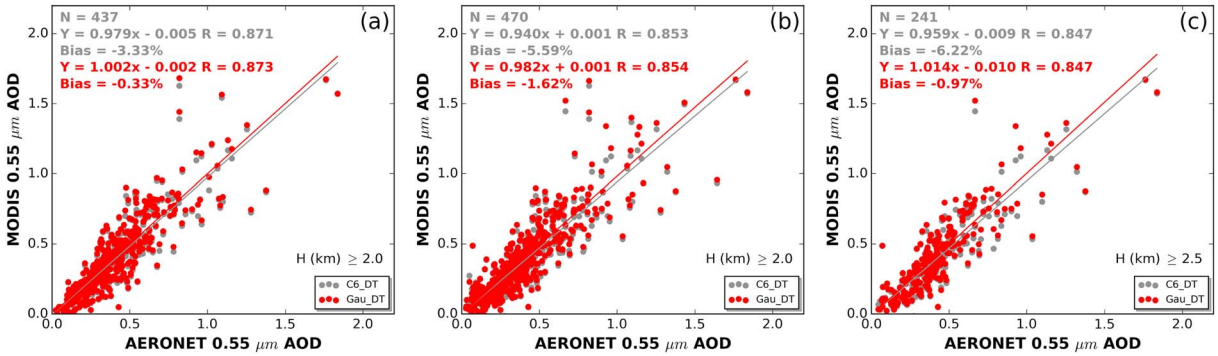

Figure 9. Scatterplot of MODIS AOD versus AERONET data. MODIS AOD of Gau_DT (red) and C6_DT (gray) present as a function of AERONET data. (a) The result with seasonal aerosol height (5 × 5°). (b, c) The results with real-time aerosol height (10 × 10 km, 75 s delay after MODIS measurements). The symbol of "H" is the mean height of aerosol layers retrieved from CALIPSO measurements.

4.1. AOD Validation With AERONET Data

The new AOD retrievals were validated using AERONET AOD data. Following the method introduced in *Petrenko et al.* [2012], MODIS AOD pixels within a circle of 25 km centered at a ground site were selected and averaged where the maximum pixels is limited to 25. AERONET measurements were averaged over a ±30 min interval centered on the Aqua satellite overpass time. A valid collocation requires that at least three MODIS pixels and two AERONET measurements present within a selected spatial-temporal window [*Levy et al.*, 2013]. For the comparison with Gau_DT, C6_DT AOD was also added. The AOD bias in the DT algorithms is evaluated as

$$\text{Bias} = (\text{DT - AERONET}) / \text{AERONET} \tag{6}$$

Three years (2008–2009) of MODIS data were collected over middle Asia (dust) and middle Africa (smoke) areas. The related information for the areas is given in Table 2. To clearly show the difference between Gau_DT and C6_DT AOD, we chose the data with the layer height >2 km. There are 437 and 470 cases collected with seasonal and real-time height data sets, respectively.

Figure 9 shows scatterplots of MODIS AOD versus AERONET data. There are some improvements on AOD retrieval bias. From Figures 9a and 9b, we can see that the bias was reduced in Gau_DT. The reductions are 3% (−3.3% to −0.3%) and 4% (−5.6% to −1.6%) with seasonal height data set and with real-time data set,

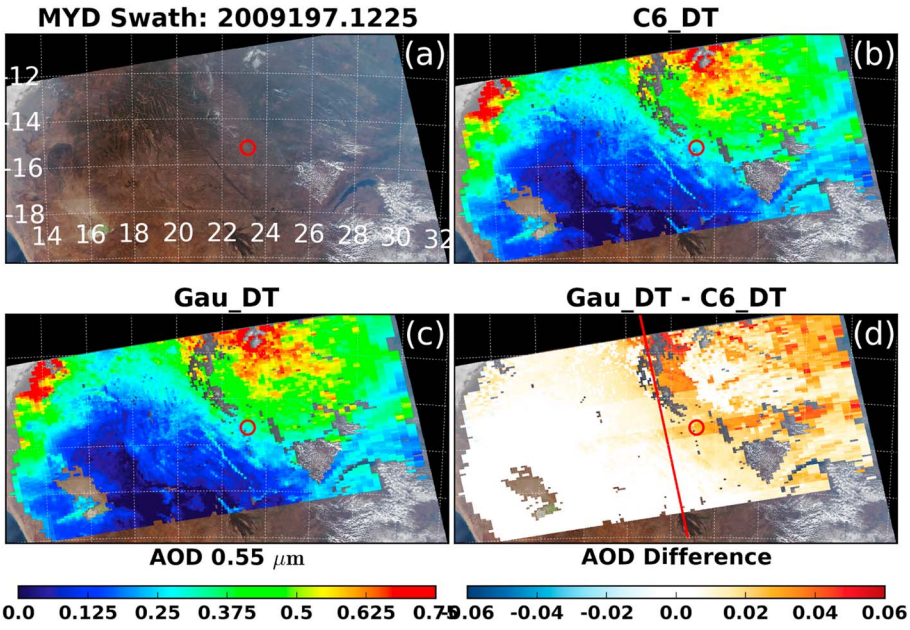

Figure 10. The smoke event over middle Africa. (a) MODIS true color image (by the combination of channels 4, 3, and 2), (b) C6_DT, (c) Gau_DT AOD, and (d) their difference overlap the MODIS image. The CALIPSO track (red line) is plotted in Figure 10d. Small red circles in Figures 10a–10d indicate the location of AERONET site Mongu (15.25°S, 23.15°E).

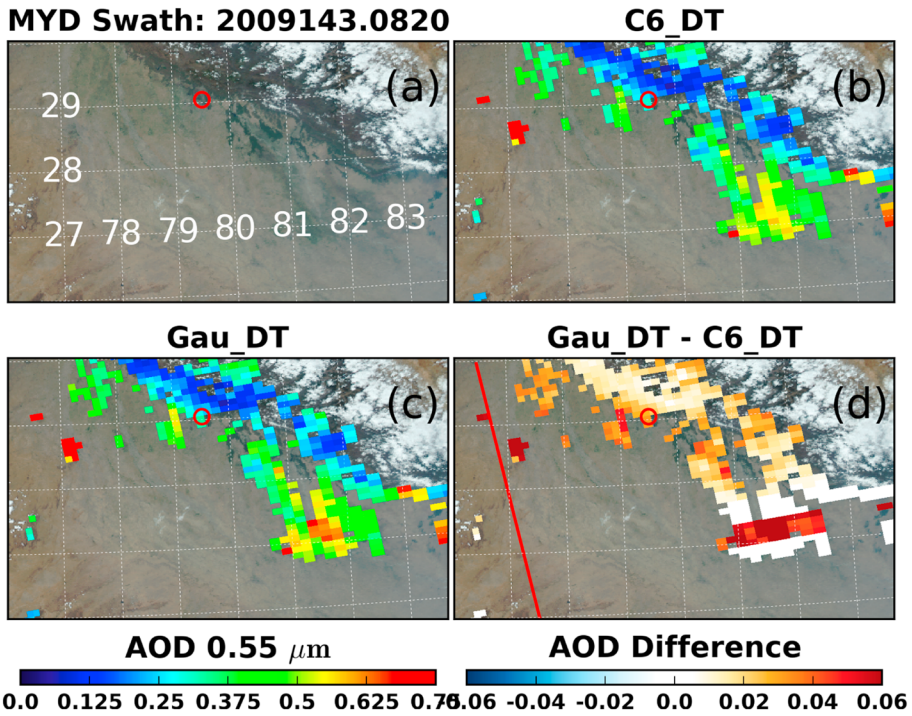

Figure 11. The dust event over middle Asia. (a–d) Similar images as in Figure 10. Small red circles in Figures 11a–11d indicate the location of AERONET site Pantnagar (29.05°N, 79.52°E).

respectively. The improvement becomes more significant for higher layers (height >2.5 km), as shown in Figure 9c. We found that the bias was reduced by 5.2% (from −6.2% to −1%) with the real-time data set. This demonstrates that Gau_DT can substantially reduce the negative bias due to the elevated aerosol layers. Nevertheless, the AOD uncertainty in Gau_DT still remains since there are trivial improvements in the correlation coefficient *R*. This uncertainty is mainly attributed to the other potential errors, i.e., errors in the spectral surface reflectance. Note that the results with the seasonal data set are not shown due to too few cases with height >2.5 km.

To get a better insight, two concrete cases of dust and smoke were selected which are located at Mongu (middle Africa) and Pantnagar (middle Asia), respectively. The results are shown with the real-time height data set.

Figure 10 shows C6_DT and Gau_DT AOD over middle Africa area, obtained on 16 July 2009. The CALIPSO track is across the MODIS image from the bottom to the top, denoted as a red line in Figure 10d. The mean height of aerosol layers is given as red line in Figure 7d. In Figure 10a, there are a lot of smoke plumes caused by fires where most plumes are originated from the eastern part (24°–32°E) and raised up to a higher level.

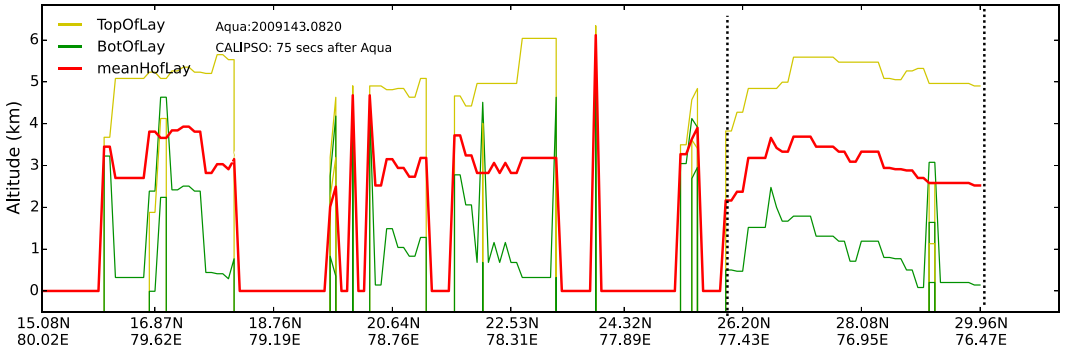

Figure 12. Dust layer information derived from CALIPSO. The data are collected on 23 May 2009 during daytime. Symbols are similar to those in Figure 7d. The two dotted lines indicate the region in Figure 11.

The climbed-up layers present much higher altitude (height >2.5 km, see Figure 7) than the assumption (height = 1.4 km) in C6_DT. As result, we can see that for the eastern part (Figure 10d) Gau_DT AOD can differ by >5% (>0.02) with C6_DT. Further, the new retrieval was found to be less biased by 5% than C6_DT against Mongu measurements. Nevertheless, for the western area, Gau_DT and C6_DT AOD do not differ too much. This is mainly because the impact due to the elevated layers is small under the oblique viewing and light aerosol loading (AOD < 0.1).

Figure 11 presents the MODIS DT AOD with the dust event, acquired on 17 July 2008. In Figures 11b and 11c, there is no AOD retrieval over large bare soil areas since the DT algorithms cannot be applied over bright surface areas. The retrievals become available over north India (dark surface area). Dust particles were well detected by both the DT algorithms (fine ratios η retrieved as 0). The dusts were from the Middle East (e.g., Iran or Sahara desert) by long distance transport, with the layer mean height ranging from 2.8 to 3.5 km (see Figure 12). Regarding this highly elevated layer, Gau_DT AOD presents significantly larger (5%–10%: 0.02–0.04) value than C6_DT. In addition, the new retrievals around Pantnagar increased by 5% (0.025) compared to C6_DT and are closer to the ground truth.

5. Conclusion

The MODIS C6_DT algorithm has successfully achieved the retrievals by using a fixed vertical profile for the aerosol layer over the globe. However, the assumption of the static vertical distribution may lead to some errors in the AOD retrieval especially for elevated aerosol layers.

In this study, a new algorithm was developed that is based on the MODIS C6_DT algorithm to account for the impact of dynamic aerosol profile in the AOD retrieval, by using MODIS and CALIPSO measurements. The relationship between the TOA reflectance and aerosol vertical profile is investigated as well as the sensitivity of the AOD retrieval to the aerosol vertical distribution under extensive conditions. We found that in the aerosol vertical profile the layer mean height is the major variable that influences the TOA reflectance. Specifically, the TOA reflectance linearly decreases with the increase of the mean height. This leads to a high sensitivity of AOD retrieval to different profiles especially when smoke or dust aerosols are observed. Normally, the use of the fixed profile (ExpH2 in C6_DT) can cause 5% to 20% errors in the retrieval for smoke or dust cases owing to the dynamic profile. To reduce these errors, the profile was parameterized into the algorithm where the profile was assumed to be a Gaussian function with the mean height as single variable. Three basic LUTs are precalculated and linearly interpolated to the measured mean height in the retrieval process.

The new algorithm was applied to smoke and dust regions with three years (2008–2010) of data. The mean height of the aerosol layer was derived from CALIPSO VFM data and resampled as seasonal ($5 \times 5°$) and real-time data sets (10×10 km), respectively. Aerosol vertical profiles are assumed to be a single layer and homogeneous spatially, i.e., $5 \times 5°$. To show the impact of the vertical profile on the retrieval, the new AOD are compared with C6_DT and validated against AERONET data.

The results show that elevated aerosol layers have a strong influence on the MODIS AOD retrieval. Generally, the elevated layers can negatively bias the retrieval by 3–5% in C6_DT. The biases are reduced to within −1.6% by the new algorithm. This becomes more significant with the increase of layer height (e.g., >2.5 km). Two specific cases were shown over AERONET site Mongu (smoke) and Pantnagar (dust).

For the elevated layers such that high altitude (3–6 km) dusts frequently occur over "dust belt" (Sahara desert, Middle East, and Taklamakan desert) during summer [*D. Liu et al.*, 2008], the new AOD retrieval can improve the estimate of the direct radiative effect by >5% when aerosol loading is ≪1.0 [*Anderson et al.*, 2005; *Levy*, 2007]. Nevertheless, we note that the AOD uncertainty remains due to the errors in spectral surface reflectance. These are subjects for further study.

Acknowledgments
We appreciate the MODIS Team for freely distributed MOD04L2 data downloaded from LAADS (https://ladsweb.nascom.nasa.gov/search) and principal investigators and managers for establishing and maintaining AERONET data. We also like to thank the CALIPSO Team for freely distributed CALIPSO levels 1 and 2 data downloaded from ASDC (https://eosweb.larc.nasa.gov/HORDERBIN/HTML_Start.cgi). We are grateful to Robert C. Levy for providing us with the source code of MODIS C6 dark target algorithm over land. Thanks to the two anonymous reviewers providing useful and helpful comments to improve the quality of the manuscript. This work was partially supported by China Scholarship Council (CSC) under the grant CSC 201206040045.

References

Anderson, T. L., et al. (2005), An "A-Train" strategy for quantifying direct climate forcing by anthropogenic aerosols, *Bull. Am. Meteorol. Soc.*, *86*(12), 1795–1809, doi:10.1175/BAMS-86-12-1795.

Carboni, E., et al. (2012), Intercomparison of desert dust optical depth from satellite measurements, *Atmos. Meas. Tech.*, *5*(8), 1973–2002, doi:10.5194/amt-5-1973-2012.

Chu, D. A., Y. J. Kaufman, G. Zibordi, J. D. Chern, J. Mao, C. Li, and B. N. Holben (2003), Global monitoring of air pollution over land from the Earth Observing System-Terra Moderate Resolution Imaging Spectroradiometer (MODIS), *J. Geophys. Res.*, *108*(D21), 4661, doi:10.1029/2002JD003179.

Dubovik, O., M. Herman, A. Holdak, T. Lapyonok, D. Taure, J. L. Deuze, F. Ducos, and A. Sinyuk (2011), Statistically optimized inversion algorithm for enhanced retrieval of aerosol properties from spectral multi-angle polarimetric satellite observations, *Atmos. Meas. Tech.*, *4*, 975–1018, doi:10.5194/amt-4-975-2011.

Eck, T. F., B. N. Holben, J. S. Reid, O. Dubovik, A. Smirnov, N. T. O'Neill, I. Slutsker, and S. Kinne (1999), Wavelength dependence of the optical depth of biomass burning, urban, and desert dust aerosols, *J. Geophys. Res.*, *104*(D24), 31,333–31,349, doi:10.1029/1999JD900923.

Engel-Cox, J. A., C. H. Holloman, B. W. Coutant, and R. M. Hoff (2004), Qualitative and quantitative evaluation of MODIS satellite sensor data for regional and urban scale air quality, *Atmos. Environ.*, *38*(16), 2495–2509, doi:10.1016/j.atmosenv.2004.01.039.

Grey, W. M. F., P. R. J. North, S. O. Los, and R. M. Mitchell (2006), Aerosol optical depth and land surface reflectance from multiangle AATSR measurements: Global validation and intersensor comparisons, *IEEE Trans. Geosci. Remote Sens.*, *44*(8), 2184–2197.

Guo, J., F. Xia, Y. Zhang, H. Liu, J. Li, M. Lou, J. He, Y. Yan, F. Wang, M. Min, and P. Zhai (2016), Impact of diurnal variability and meteorological factors on the $PM_{2.5}$–AOD relationship: Implications for $PM_{2.5}$ remote sensing, *Environ. Pollut.*, *221*, 94–104, doi:10.1016/j.envpol.2016.11.043.

Herman, M., J.-L. Deuzé, A. Marchand, B. Roger, and P. Lallart (2005), Aerosol remote sensing from POLDER/ADEOS over the ocean: Improved retrieval using a nonspherical particle model, *J. Geophys. Res.*, *110*, D10S02, doi:10.1029/2004JD004798.

Hoff, R. M., and S. A. Christopher (2009), Remote sensing of particulate pollution from space: Have we reached the promised land?, *J. Air Waste Manage. Assoc.*, *59*(6), 645–675, doi:10.3155/1047-3289.59.6.645.

Hsu, N. C., S.-C. Tsay, M. D. King, and J. R. Herman (2004), Aerosol properties over bright-reflecting source regions, *IEEE Trans. Geosci. Remote Sens.*, *42*(3), 557–569, doi:10.1109/TGRS.2004.824067.

Hsu, N. C., S. C. Tsay, M. D. King, and J. R. Herman (2006), Deep blue retrievals of Asian aerosol properties during acE-Asia, *IEEE Trans. Geosci. Remote Sens.*, *44*(11), 3180–3195, doi:10.1109/TGRS.2006.879540.

Hsu, N. C., M.-J. Jeong, C. Bettenhausen, A. M. Sayer, R. Hansell, C. S. Seftor, J. Huang, and S.-C. Tsay (2013), Enhanced Deep Blue aerosol retrieval algorithm: The second generation, *J. Geophys. Res. Atmos.*, *118*, 9296–9315, doi:10.1002/jgrd.50712.

Huang, J., J. Guo, F. Wang, Z. Liu, M.-J. Jeong, H. Yu, and Z. Zhang (2015), CALIPSO inferred most probable heights of global dust and smoke layers, *J. Geophys. Res. Atmos.*, *120*, 5085–5100, doi:10.1002/2014JD022898.

Intergovernmental Panel on Climate Change (IPCC) (2013), *Working Group I Contribution to the IPCC Fifth Assessment Report (AR5) Climate Change 2013: The Physical Science Basis*, Intergovernmental Panel on Climate Change, Geneva, Switzerland.

Kahn, R. A., B. J. Gaitley, M. J. Garay, D. J. Diner, T. F. Eck, A. Smirnov, and B. N. Holben (2010), Multiangle Imaging SpectroRadiometer global aerosol product assessment by comparison with the Aerosol Robotic Network, *J. Geophys. Res.*, *115*, D23209, doi:10.1029/2010JD014601.

Kaufman, Y. J., D. Tanré, L. A. Remer, E. F. Vermote, A. Chu, and B. N. Holben (1997), Operational remote sensing of tropospheric aerosol over land from EOS moderate resolution imaging spectroradiometer, *J. Geophys. Res.*, *102*(D14), 17,051–17,067, doi:10.1029/96JD03988.

Kaufman, Y. J., D. Tanré, and O. Boucher (2002), A satellite view of aerosols in the climate system, *Nature*, *419*(6903), 215–223, doi:10.1038/nature01091.

Keller, J., S. Bojinski, and A. S. H. Prevot (2007), Simultaneous retrieval of aerosol and surface optical properties using data of the Multi-angle Imaging SpectroRadiometer (MISR), *Remote Sens. Environ.*, *107*(1-2), 120–137, doi:10.1016/j.rse.2006.07.020.

Kokhanovsky, A. A., et al. (2010), The inter-comparison of major satellite aerosol retrieval algorithms using simulated intensity and polarization characteristics of reflected light, *Atmos. Meas. Tech.*, *3*(4), 909–932, doi:10.5194/amt-3-909-2010.

Kokhanovsky, A. A., et al. (2015), Space-based remote sensing of atmospheric aerosols: The multi-angle spectro-polarimetric frontier, *Earth Sci. Rev.*, *145*, 85–116, doi:10.1016/j.earscirev.2015.01.012.

Lee, J., N. C. Hsu, C. Bettenhausen, A. M. Sayer, C. J. Seftor, and M.-J. Jeong (2015), Retrieving the height of smoke and dust aerosols by synergistic use of VIIRS, OMPS, and CALIOP observations, *J. Geophys. Res. Atmos.*, *120*, 8372–8388, doi:10.1002/2015JD023567.

Levy, R. C. (2007), Retrieval of tropospheric aerosol properties over land from inversion of visible and near-infrared spectral reflectance: Application over Maryland, dissertation, sec. 2, chap. 9, Univ. of Maryland, College Park, Md.

Levy, R. C., L. A. Remer, J. V. Martins, Y. J. Kaufman, A. Plana-Fattori, J. Redemann, and B. Wenny (2005), Evaluation of the MODIS aerosol retrievals over ocean and land during CLAMS, *J. Atmos. Sci.*, *62*(4), 974–992, doi:10.1175/JAS3391.1.

Levy, R. C., L. A. Remer, S. Mattoo, E. F. Vermote, and Y. J. Kaufman (2007a), Second-generation operational algorithm: retrieval of aerosol properties over land from inversion of Moderate Resolution Imaging Spectroradiometer spectral reflectance, *J. Geophys. Res.*, *112*, D13211, doi:10.1029/2006JD007811.

Levy, R. C., L. A. Remer, and O. Dubovik (2007b), Global aerosol optical properties and application to Moderate Resolution Imaging Spectroradiometer aerosol retrieval over land, *J. Geophys. Res.*, *112*, D13210, doi:10.1029/2006JD007815.

Levy, R. C., L. A. Remer, R. G. Kleidman, S. Mattoo, C. Ichoku, R. Kahn, and T. F. Eck (2010), Global evaluation of the Collection 5 MODIS dark-target aerosol products over land, *Atmos. Chem. Phys.*, *10*(21), 10,399–10,420, doi:10.5194/acp-10-10399-2010.

Levy, R. C., S. Mattoo, L. A. Munchak, L. A. Remer, A. M. Sayer, F. Patadia, and N. C. Hsu (2013), The Collection 6 MODIS aerosol products over land and ocean, *Atmos. Meas. Tech.*, *6*(11), 2989–3034, doi:10.5194/amt-6-2989-2013.

Li, Z., X. Zhao, R. Kahn, M. Mishchenko, L. Remer, K.-H. Lee, M. Wang, I. Laszlo, T. Nakajima, and H. Maring (2009), Uncertainties in satellite remote sensing of aerosols and impact on monitoring its long-term trend: A review and perspective, *Ann. Geophys.*, *27*(7), 2755–2770, doi:10.5194/angeo-27-2755-2009.

Liu, D., Z. Wang, Z. Liu, D. Winker, and C. Trepte (2008), A height resolved global view of dust aerosols from the first year CALIPSO lidar measurements, *J. Geophys. Res.*, *113*, D16214, doi:10.1029/2007JD009776.

Liu, Z., et al. (2008), CALIPSO lidar observations of the optical properties of Saharan dust: A case study of long-range transport, *J. Geophys. Res.*, *113*, D07207, doi:10.1029/2007JD008878.

Lyapustin, A., J. Martonchik, Y. Wang, I. Laszlo, and S. Korkin (2011a), Multiangle Implementation of Atmospheric Correction (MAIAC): 1. Radiative transfer basis and look-up tables, *J. Geophys. Res.*, *116*, D03210, doi:10.1029/2010JD014985.

Lyapustin, A., Y. Wang, I. Laszlo, R. Kahn, S. Korkin, L. Remer, R. Levy, and J. S. Reid (2011b), Multiangle Implementation of Atmospheric Correction (MAIAC): 2. Aerosol algorithm, *J. Geophys. Res.*, *116*, D03211, doi:10.1029/2010JD014986.

Martonchik, J., D. Diner, K. Crean, and M. Bull (2002), Regional aerosol retrieval results from MISR, *IEEE Trans. Geosci. Remote Sens.*, *40*(7), 1520–1531, doi:10.1109/TGRS.2002.801142.

Martonchik, J. V., D. J. Diner, R. A. Kahn, T. P. Ackerman, M. M. Verstraete, B. Pinty, and H. R. Gordon (1998), Techniques for the retrieval of aerosol properties over land and ocean using multiangle imaging, *IEEE Trans. Geosci. Remote Sens.*, *36*(4), 1212–1227, doi:10.1109/36.701027.

Martonchik, J. V., R. A. Kahn, and D. J. Diner (2009), Retrieval of aerosol properties over land using MISR observations, in *Satellite Aerosol Remote Sensing Over Land*, pp. 267–293, Springer, Berlin.

Mishchenko, M. I., I. V. Geogdzhayev, B. Cairns, W. B. Rossow, and A. A. Lacis (1999), Aerosol retrievals over the ocean by use of channels 1 and 2 AVHRR data: Sensitivity analysis and preliminary results, *Appl. Opt.*, *38*(36), 7325, doi:10.1364/AO.38.007325.

Myhre, G. (2009), Consistency between satellite-derived and modeled estimates of the direct aerosol effect, *Science*, *325*(5937), 187–190, doi:10.1126/science.1174461.

Nicolantonio, W. D., A. Cacciari, E. Bolzacchini, L. Ferrero, M. Volta, and E. Pisoni (2007), MODIS aerosol optical properties over north Italy for estimating surface-level $PM_{2.5}$, in *Proceedings Envisat Symposium*, pp. 3–27, ESA SP, Number SP-636, Eur. Space Agency, (Spec. Publ.), Montreux, Switzerland.

North, P. R. J. (2002), Estimation of aerosol opacity and land surface bidirectional reflectance from ATSR-2 dual-angle imagery: Operational method and validation, *J. Geophys. Res.*, *107*(D12), 4149, doi:10.1029/2000JD000207.

North, P. R. J., S. A. Briggs, S. E. Plummer, and J. J. Settle (1999), Retrieval of land surface bidirectional reflectance and aerosol opacity from ATSR-2 multiangle imagery, *IEEE Trans. Geosci. Remote Sens.*, *37*(1), 526–537, doi:10.1109/36.739106.

Petrenko, M., C. Ichoku, and G. Leptoukh (2012), Multi-sensor Aerosol Products Sampling System (MAPSS), *Atmos. Meas. Tech.*, *5*(5), 913–926, doi:10.5194/amt-5-913-2012.

Remer, L. A., et al. (2005), The MODIS aerosol algorithm, products, and validation, *J. Atmos. Sci.*, *62*(4), 947–973, doi:10.1175/JAS3385.1.

Sayer, A. M., N. C. Hsu, C. Bettenhausen, M.-J. Jeong, B. N. Holben, and J. Zhang (2012), Global and regional evaluation of over-land spectral aerosol optical depth retrievals from SeaWiFS, *Atmos. Meas. Tech.*, *5*(7), 1761–1778, doi:10.5194/amt-5-1761-2012.

Sayer, A. M., N. C. Hsu, C. Bettenhausen, and M.-J. Jeong (2013), Validation and uncertainty estimates for MODIS Collection 6 Deep Blue aerosol data, *J. Geophys. Res. Atmos.*, *118*, 7864–7872, doi:10.1002/jgrd.50600.

Sayer, A. M., N. C. Hsu, C. Bettenhausen, M.-J. Jeong, and G. Meister (2015), Effect of MODIS Terra radiometric calibration improvements on Collection 6 Deep Blue aerosol products: Validation and Terra/Aqua consistency, *J. Geophys. Res. Atmos.*, *120*, 12,157–12,174, doi:10.1002/2015JD023878.

Sayer, A. M., N. C. Hsu, C. Bettenhausen, J. Lee, J. Redemann, B. Schmid, and Y. Shinozuka (2016), Extending "Deep Blue" aerosol retrieval coverage to cases of absorbing aerosols above clouds: Sensitivity analysis and first case studies, *J. Geophys. Res. Atmos.*, *121*, 4830–4854, doi:10.1002/2015JD024729.

Stowe, L. L., A. M. Ignatov, and R. R. Singh (1997), Development, validation, and potential enhancements to the second-generation operational aerosol product at the National Environmental Satellite, Data, and Information Service of the National Oceanic and Atmospheric Administration, *J. Geophys. Res.*, *102*(D14), 16,923–16,934, doi:10.1029/96JD02132.

Tanré, D., F. M. Bréon, J. L. Deuzé, O. Dubovik, F. Ducos, P. François, P. Goloub, M. Herman, A. Lifermann, and F. Waquet (2011), Remote sensing of aerosols by using polarized, directional and spectral measurements within the A-Train: The PARASOL mission, *Atmos. Meas. Tech.*, *4*(7), 1383–1395, doi:10.5194/amt-4-1383-2011.

Tao, M., L. Chen, Z. Wang, J. Tao, H. Che, X. Wang, and Y. Wang (2015), Comparison and evaluation of the MODIS Collection 6 aerosol data in China, *J. Geophys. Res. Atmos.*, *120*, 6992–7005, doi:10.1002/2015JD023360.

Thomas, G. E., C. A. Poulsen, A. M. Sayer, S. H. Marsh, S. M. Dean, E. Carboni, R. Siddans, R. G. Grainger, and B. N. Lawrence (2009), The GRAPE aerosol retrieval algorithm, *Atmos. Meas. Tech.*, *2*(2), 679–701, doi:10.5194/amt-2-679-2009.

Vaughan, M. A., D. M. Winker, and K. A. Powell (2005), *CALIOP Algorithm Theoretical Basis Document Part 2: Feature Detection and Layer Properties Algorithms*, NASA Langley Res. Cent., Hampton, Va.

Winker, D. M., C. A. Hostetler, M. A. Vaughan, and A. H. Omar (2006), *CALIOP Algorithm Theoretical Basis Document Part 1: CALIOP Instrument, and Algorithms Overview*, NASA Langley Res. Cent., Hampton, Va.

Wu, Y., J. Guo, X. Zhang, X. Tian, J. Zhang, Y. Wang, J. Duan, and X. Li (2012), Synergy of satellite and ground based observations in estimation of particulate matter in eastern China, *Sci. Total Environ.*, *433*, 20–30, doi:10.1016/j.scitotenv.2012.06.033.

Wu, Y., M. de Graaf, and M. Menenti (2016a), The sensitivity of AOD retrieval to aerosol type and vertical distribution over land with MODIS data, *Remote Sens.*, *8*(9), 765, doi:10.3390/rs8090765.

Wu, Y., M. de Graaf, and M. Menenti (2016b), Improved MODIS Dark Target aerosol optical depth algorithm over land: Angular effect correction, *Atmos. Meas. Tech.*, *9*(11), 5575–5589, doi:10.5194/amt-9-5575-2016.

Xu, H., J. Guo, X. Ceamanos, J.-L. Roujean, M. Min, and D. Carrer (2016), On the influence of the diurnal variations of aerosol content to estimate direct aerosol radiative forcing using MODIS data, *Atmos. Environ.*, *141*, 186–196, doi:10.1016/j.atmosenv.2016.06.067.